JGR Atmospheres

RESEARCH ARTICLE
10.1029/2021JD035013

Blue Flashes as Counterparts to Narrow Bipolar Events: The Optical Signal of Shallow In-Cloud Discharges

Dongshuai Li[1], Alejandro Luque[1], F. J. Gordillo-Vázquez[1], Feifan Liu[2], Gaopeng Lu[2], Torsten Neubert[3], Olivier Chanrion[3], Baoyou Zhu[2], Nikolai Østgaard[4], and Víctor Reglero[5]

[1]Instituto de Astrofísica de Andalucía (IAA), CSIC, Granada, Spain, [2]CAS Key Laboratory of Geospace Environment, School of Earth and Space Sciences, University of Science and Technology of China, Hefei, China, [3]National Space Institute, Technical University of Denmark (DTU Space), Kongens Lyngby, Denmark, [4]Birkeland Centre for Space Science, Department of Physics and Technology, University of Bergen, Bergen, Norway, [5]Image Processing Laboratory, University of Valencia, Valencia, Spain

Key Points:

- Negative-polarity narrow bipolar events are typically associated with extended optical sources at the edge of a thundercloud
- Thermal emissions in the oxygen 777 nm band are absent or very weak, indicating non-thermal processes
- The optical energy in the 337 nm band is about 10^4 J, which requires around 10^9 streamers

Supporting Information:

Supporting Information may be found in the online version of this article.

Correspondence to:

D. Li and A. Luque,
dsl@iaa.es;
aluque@iaa.es

Citation:

Li, D., Luque, A., Gordillo-Vázquez, F. J., Liu, F., Lu, G., Neubert, T., et al. (2021). Blue flashes as counterparts to narrow bipolar events: The optical signal of shallow in-cloud discharges. *Journal of Geophysical Research: Atmospheres*, *126*, e2021JD035013. https://doi.org/10.1029/2021JD035013

Received 5 APR 2021
Accepted 14 JUN 2021

Abstract Narrow Bipolar Events (NBEs) are powerful radio emissions from thunderstorms, which have been recently associated with blue optical flashes on cloud tops and attributed to extensive streamer electrical discharges named fast breakdown. Combining data obtained from a thunderstorm over South China by the space-based Atmosphere Space Interactions Monitor, the Vaisala GLD360 global lightning network and very low frequency/low frequency radio detectors, here we report and analyze for the first time the optical emissions of blue luminous events associated with negative NBEs and located at the top edge of a thundercloud. These emissions are weakly affected by scattering from cloud droplets, allowing us to estimate the source extension and optical energy involved in the process. The optical energy in the 337-nm band emitted by fast breakdown is about 10^4 J, which involves around 10^9 streamer initiation events.

Plain Language Summary Installed on the International Space Station, the Atmosphere-Space Interactions Monitor is designed to observe Earth thunderstorms from space. Often it detects bursts of blue light emerging from active thunderclouds. These detections have been previously linked to radio signals named narrow bipolar events (NBEs) that are routinely detected during a thunderstorm. Here we analyze the blue flashes from a storm that profusely produced negative-polarity NBEs. The optical signal can be understood as being produced by extended events close to the cloud top and we show that it is consistent with the barely understood electrical discharge process called fast breakdown that involves a huge number of thin, bright filaments called streamers.

1. Introduction

Blue luminous events (hereafter, BLUEs), such as blue jets and blue starters, are transient electrical phenomena that occur in active thunderstorms and are characterized by optical signals strongly dominated by the blue range of the spectrum and lasting from about one millisecond to hundreds of milliseconds. They were first reported by Wescott et al. (1995, 1996) in the framework of the Sprites 1994 aircraft campaign. After these initial reports, BLUEs have been observed and investigated mainly from space-based platforms: for example, from black-and-white camera of the Space Shuttle (Boeck et al., 1998), from the limb-pointing Imager of Sprites/Upper Atmospheric Lightning (ISUAL) onboard FORMOSAT-2 (Chou et al., 2011, 2018; Kuo et al., 2005), from off-the-shelf cameras on the International Space Station (ISS) (Chanrion et al., 2017) and, most recently, from the Modular Multispectral Imaging Array (MMIA) of the Atmosphere-Space Interactions Monitor (ASIM) onboard the ISS since April 2, 2018 (Neubert et al., 2021; Soler et al., 2020). BLUEs can also be observed from the ground, as reported by Edens (2011), but this is complicated due to Rayleigh scattering and extinction by intervening clouds.

As we define them here, BLUEs comprise several phenomena. Blue jets normally emerge out of the cloud top and reach altitudes about 40–50 km at speeds of the order of 100 km/s (Wescott et al., 2001). Blue starters terminate at lower altitudes, typically around 18 km but sometimes up to 25 km and advance with velocities 10–100 km/s (Wescott et al., 1996); they are often described as initial phases of blue jets (Pasko, 2008) and hence their name. Other types of BLUEs have also been reported, including small blue

surface discharges (sometimes called *blue glimpses*) that appear to "dance" on the upper layer of the cloud at a rate of about 120 per min (Chanrion et al., 2017) and the *gnomes* that emerge directly from the cloud top within ∼1 km, similar to blue starters, but with brighter and more uniform optical emission and much more compact shape (Lyons et al., 2003). We do not classify *Giant jets*, which travel from cloud tops to the lower ionosphere, as BLUEs, since they involve significative emissions in the 777.4-nm band (van der Velde et al., 2019).

Each of these types of phenomena exhibits a different morphology but they likely share common physical processes. The blue color indicates the presence of electron-impact excitation of molecular nitrogen (Gordillo-Vázquez & Pérez-Invernón, 2021; Pasko, 2008; Surkov & Hayakawa, 2020) and the weak or absent atomic oxygen line at 777.4 nm, indicates that air does not reach high temperatures, typically associated with lightning leaders at ground level. This points to streamer coronas being the key component of BLUEs, a conclusion supported by the close association between BLUEs and narrow bipolar events (NBEs) (F. Liu et al., 2018; Soler et al., 2020), which are radio emissions also attributed to corona discharges in thunderclouds (N. Liu et al., 2019; Rison et al., 2016; Tilles et al., 2019). It is thus likely that both BLUEs and NBEs are electromagnetic manifestations of large streamer coronas (or *fast breakdown*, a term coined by Rison et al., 2016 that we also adopt here).

Some distinctive features of each type of BLUE arise from their extension and their location inside the thundercloud. For example, Soler et al. (2020) analyzed a set of 10 BLUEs associated with positive NBEs and at a considerable depth inside the cloud, presumably between the main negative and the upper positive charge region of the cloud. As these events are deeply buried in the cloud, the scattering by cloud droplets and ice crystals blurs their image as observed from above, resulting in a diffuse blob that can be identified with the blue glimpses reported by Chanrion et al. (2017).

Here, we focus on events that are close to the cloud top, perhaps partially outside the cloud. This location suggests an origin between the upper positive region of the cloud and the negatively charged screening layer, and this is supported by radio detections that associate these events with negative-polarity NBEs (positive charges moving upward) (Lyu et al., 2015; Smith et al., 1999; Wu et al., 2012). Because the emissions come from close to the cloud top, optical radiation is less affected by scattering, leading to a more robust inferrence of source characteristics. This allows us to compare to radio observations of fast breakdown.

2. Instruments and Observations

The MMIA is a component of the ASIM, a mission launched on April 2, 2018 and installed on the ISS (Chanrion et al., 2019; Neubert et al., 2019). MMIA observes in ultraviolet and near-infrared wavelengths, points towards the nadir and contains three photometers and two cameras. The three photometers, with a temporal sampling rate of 100 ksamples/s, include one in the UV band at 180–230 nm, and two others sensitive to the same wavelengths as two installed cameras: in the near-UV at the strongest spectral line of the nitrogen second positive system (337 nm) and at the strongest lightning emission line, OI (777.4 nm). The spatial resolution of the cameras is around 400 × 400 m at the nadir point and their integration time is 83.3 ms.

On the evening of August 7, 2019, above an intense localized thunderstorm over Southern China, there were eight BLUEs simultaneously detected by MMIA, the ground-based Vaisala GLD360 global lightning network and the ground-based very low frequency (VLF)/low frequency (LF) sensor at Guangzhou (see Table 1 for further details). All of them were detected by MMIA's photometer and camera filtered at 337 nm; some events had a detectable signal in the 180–230 nm photometer but there was no signal in the 777.4 nm photometer and camera at the 3σ confidence level. Depending on the event this implies that the 777.4-nm flux was at least between 50 and 300 times weaker than the 337-nm flux (see Figure A1 and the text there in Appendix A for more details). The rise times of the events in the 337 nm photometer are below 56 μs, with the shortest of them being unresolved by the 10 μs sampling time of the photometer. The peak brightness ranges from 20 to 140 $\mu W/m^2$, which is among the brightest signals detected by MMIA. The brightness and quick rise of the events indicate that they originate close to the cloud tops

Table 1
The Eight BLUEs Simultaneously Detected by MMIA, Ground-Based Vaisala GLD360 Global Lightning Network and the Ground-Based VLF/LF Sensor at Guangzhou

ID	Date (Year/ Month/Day)	MMIA time UTC(Source)	MMIA corrected time UTC(Source)	GLD360 time UTC(Source)	VLF/LF time UTC(Source)	Rise time (μs)[a]	Time duration (μs)[b]	Peak brightness (μW/m^2)
1	Aug 07, 2019	13:05:56.9362	13:05:56.9595	13:05:56.9594	13:05:56.9594	31	370	20.11
2	Aug 07, 2019	13:05:58.6317	13:05:58.6550	13:05:58.6549	13:05:58.6549	8	200	142.18
3	Aug 07, 2019	13:06:01.7568	13:06:01.7801	13:06:01.7800	13:06:01.7799	56	760	40.61
4	Aug 07, 2019	13:06:09.5668	13:06:09.5730	13:06:09.5722	13:06:09.5723	9	400	97.88
5	Aug 07, 2019	13:06:16.6329	13:06:16.6391	–	13:06:16.6384	13	910	45
6	Aug 07, 2019	13:06:20.9670	13:06:20.9732	13:06:20.9726	13:06:20.9726	14	490	120.30
7	Aug 07, 2019	13:06:30.4934	13:06:30.4996	–	13:06:30.4993	13	330	46.48
8	Aug 07, 2019	13:06:31.6557	13:06:31.6619	13:06:31.6616	13:06:31.6615	13	240	39.96

Note. All the detection times have been corrected to the time with respect to the BLUEs source locations.
Abbreviations: BLUEs, blue luminous events; LF, low frequency; MMIA, Modular Multispectral Imaging Array; VLF, very low frequency.
[a]Rise time is calculated using the linear interpolation by taking the time for the amplitude of a photometer signal to rise from 10% to 90%. Note that the sampling time is 10 μs so the rise is unresolved in several events. [b]Time duration is calculated using the linear interpolation by the time interval for the amplitude of a photometer signal to rise from 10% and fall to 10%.

or perhaps slightly above them. Note that below, we show that most of the emissions were partially scattered by the cloud and that the photometer light curve is not indicative of the true source duration.

We sketch the context of the eight BLUEs in Figure 1 which, in panels (a) and (b), plots the intra-cloud (IC) and cloud-to-ground (CG) flashes and the eight BLUEs superimposed on the cloud top height (CTH) provided by the Fengyun-4A (FY-4A) satellite (Yang et al., 2017) for the time period from 13:04:00 to 13:07:00 UTC. During these three minutes, there were 522 lightning events with 240 CG and 282 IC flashes reported by GLD360 (see Figure 1). Two of the BLUE events (with ID 5 and 7) were missing from GLD360 so for all the BLUEs, we use the location provided by the lightning location systems (LLSs) in Guangzhou province (Chen et al., 2012).

The absolute timing uncertainty of MMIA is on the order of tens of milliseconds but we can correct the MMIA times to sub-millisecond accuracy by comparing flash times provided by GLD360 to MMIA 777.4 nm-pulses. In our case, we found that the systematic time shift with respect to the ground-based measurements experienced a time adjustment at around 13:06:07, the time corrections before and after the time adjustment are -23.3 ± 0.3 ms and -6.2 ± 0.5 ms, respectively (see Figure B1 in Appendix B for further details). Note that the time shift −23.3 ms is similar to the estimations for other thunderstorms such as the −28.7 ms inferred by Soler et al. (2020) or the −16.37 ms from Neubert et al. (2021).

With this time correction we find that each of the eight BLUEs has a radio signal that, when back-propagated to the source, is within 0.7 ms of the optical peak. All VLF/LF waveforms of the BLUEs were unambiguously classified as negative NBEs measured by the vertical electric field antenna (frequency bandwidth 800 Hz–400 kHz) located about 105 km away at Guangzhou station of Jianghuai Area Sferic Array (Qin et al., 2015; F. Liu et al., 2018).

Figure 1 shows in panels (c) and (d) a composition of all camera images for the BLUE events (always from the 337 nm-filtered camera). To produce this picture we have added the projection of each of the eight MMIA images into the Earth surface according to coordinates introduced by the ASIM pipeline. The resulting locations differ noticeably from those provided by LLSs and the distribution is more spread out. We attribute this to uncertainties in the camera orientation. Note also that several of the images exhibit

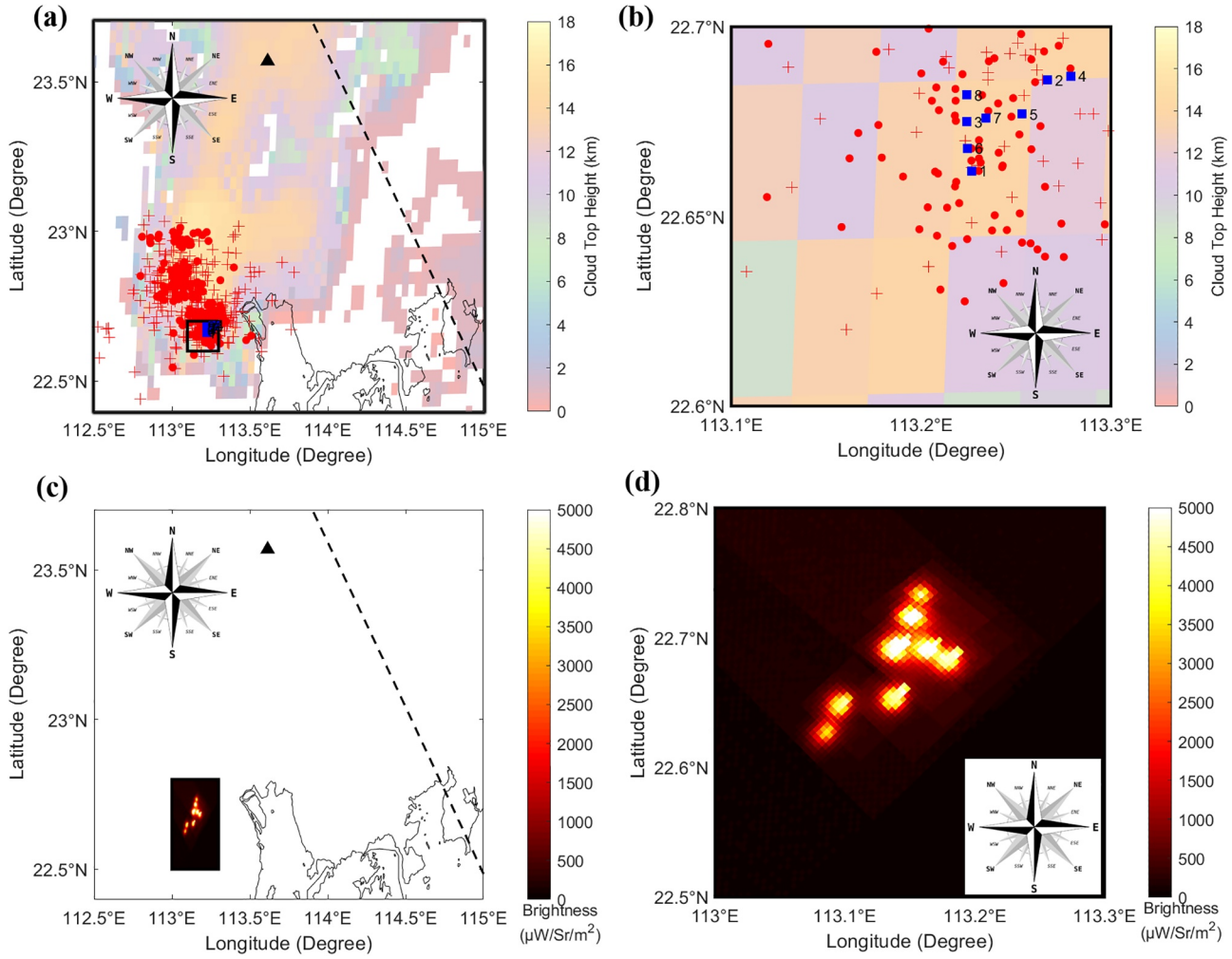

Figure 1. Distribution of the cloud-to-ground (CG)/intra-cloud (IC) lightning and eight blue luminous events (BLUEs) along with Cloud Top Height (CTH) at the time period from 13:04:00 to 13:07:00 UTC (a) and the zoom of its black rectangular region (b) (Red dots: CG lightning detected by GLD360, Red crosses: IC lightning detected by GLD360 and Blue squares: BLUEs detected by LLSs); eight BLUEs images detected in the 337 nm filtered camera of Modular Multispectral Imaging Array (c) and the zoom (d). The ground-based VLF/LF sensor at Guangzhou is shown as black triangle. The footprints of Atmosphere-Space Interactions Monitor are shown in black dashed line.

a sharp peak that appears to emerge from the middle of the diffuse blob: this is a blooming artifact of the CCD camera.

To understand better the relation between the BLUE emissions and their parent thunderstorm, we examined the progression of the cloud Top Blackbody Brightness temperature (TBB in *K*) provided by the Himawari-8 satellite (Bessho et al., 2016) with ten-minute resolution. Figure 2 displays the TBB around the time of our detections. The BLUE events originated from the boundary of a rapidly evolving thunderstorm cell. This suggests that rapid turbulent mixing of the screening layer plays a role in the inception of fast breakdown (Krehbiel et al., 2008; Lyons et al., 2003) or the occurrence of groups of localized NBEs is associated with dynamically intense convection (Bandara et al., 2021). Note that the cloud top heights provided by FY-4A that we use here are likely underestimates 2–3 km comparing with radar data (B. Liu et al., 2021; F. Liu et al., 2021). Since the negative NBEs are usually associated with deep convection and detected in overshooting cloud tops (F. Liu et al., 2018; Wu et al., 2013), which might also cause uncertainties.

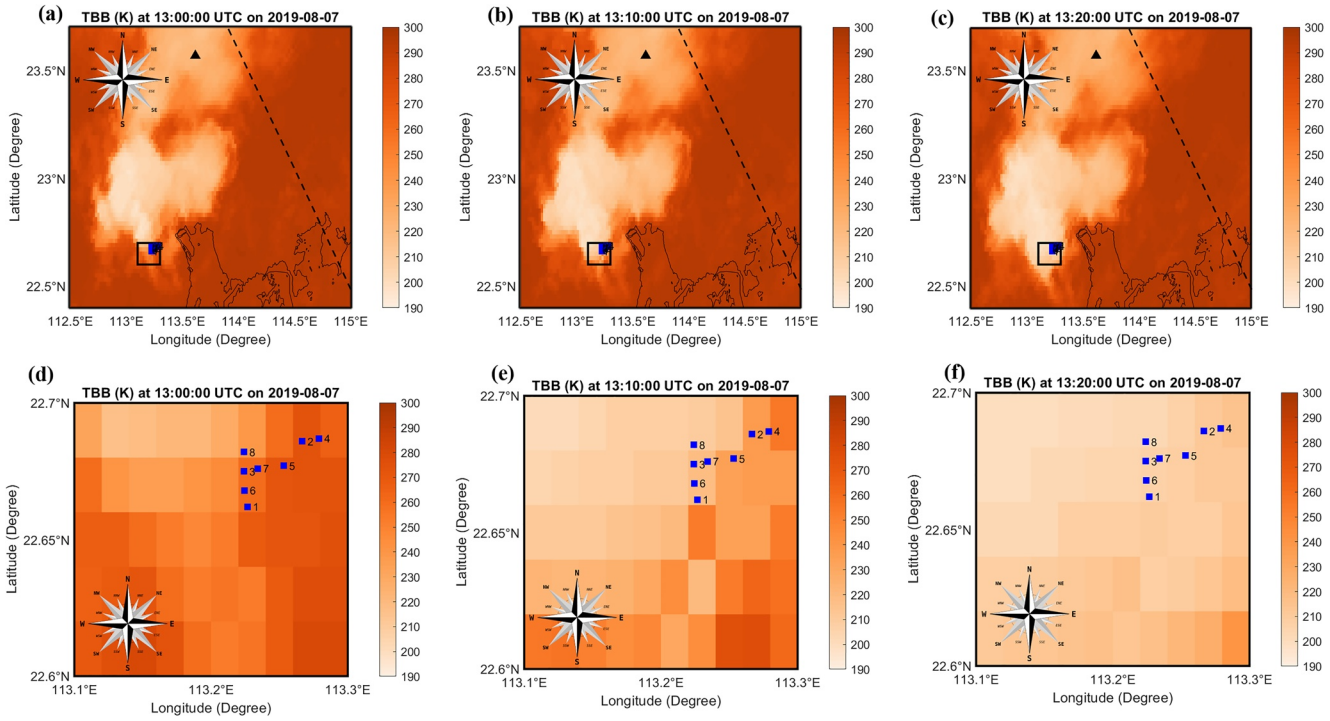

Figure 2. Cloud top blackbody brightness temperature (TBB, in K) and the zoom of its black rectangular region provided by Himawari-8 at 13:00:00 UTC (a) and (d), at 13:10:00 UTC (b) and (e), at 13:20:00 UTC (c) and (f). The ground-based VLF/LF sensor at Guangzhou is shown as black triangle. The footprints of Atmosphere-Space Interactions Monitor are shown in black dashed line.

3. Light-Scattering Model

To better understand the MMIA observations we compare them now to a simple model where the light source is a thin, straight, uniformly bright segment and the cloud is homogeneous with a planar upper boundary. We neglect the intrinsic duration of the source, assuming that all light is emitted instantaneously. This is consistent with the source durations for NBEs of about 10 microseconds estimated by Rison et al. (2016), which is much shorter than the signal waveforms that last several hundred microseconds. The propagation velocity of the discharges is thus unresolved in our analysis.

Because photons can be scattered many times before they exit the cloud, an impulsive optical flash results in a temporally stretched light curve. To understand this curve, we start with the expression for a point-like source buried in the cloud. Using the diffusion approximation for the propagation of photons inside the cloud proposed by Koshak et al. (1994) and Soler et al. (2020) gave an analytical expression for this curve, which was derived in more detail by Luque et al. (2020). Adopting the normalization and the notation of the latter the photon flux exiting the cloud top has the following expression valid for $t > 0$, with the time origin being the moment of light emission:

$$\Gamma(t) = NF(t) = \frac{Ne^{-t/\tau_A - \tau_D/t}}{\pi^{1/2}\tau_D}\left(\frac{t}{\tau_D}\right)^{-3/2}, \quad (1)$$

where $F(t)$ is the flux per photon in the source, N is the total number of source photons, τ_A is the mean absorption time of the photons inside the cloud and $\tau_D = L^2/4D$ is, given a diffusion coeffcient D, the characteristic time of diffusion for the distance L between the source and the cloud top. The derivation of these magnitudes from the microscopic properties of the cloud is given by Koshak et al. (1994) and reviewed by Luque et al. (2020). For a distant observer, differences in light travel time from different points in the cloud

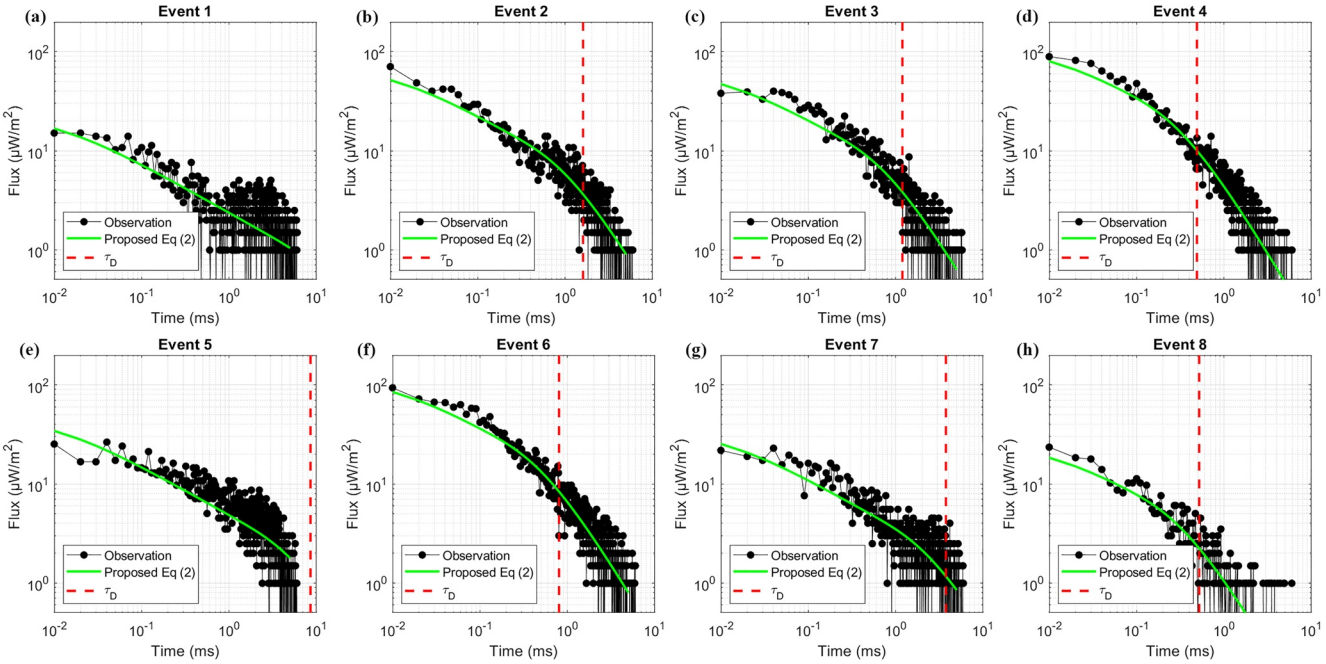

Figure 3. Comparison between Modular Multispectral Imaging Array observed photometer signals and those calculated by using the proposed Equation 2 over the time after peak on a logarithmic scale. The best-fit cutoff time τ_D is shown in red dashed line.

are not significant so one can reinterpret the time in Equation 1 with $t = 0$ being the arrival time of an unscattered photon.

3.1. Length of the Optical Source

To obtain the light curve for an extended source that spans altitudes from the cloud top to a maximum depth L_0 we integrate $(N/L_0)F(t)dL$ in Equation 1 from 0 to L_0 (the factor N/L_0 is the linear density of source photons, assumed uniform). The result is

$$\Gamma_L(t) = \frac{N}{L_0}\left(\frac{D}{t}\right)^{1/2}\left(1 - e^{-\tau_D/t}\right)e^{-t/\tau_A}, \tau_D = L_0^2 / 4D. \quad (2)$$

Note that this expression disregards any part of the source above the cloud top. Some photons emitted outside the cloud propagate directly to the detector and others are back-scattered by the upper cloud surface after a small number of scattering events. These emissions have an effect only on a few data points in a photometer with a 10 μs time resolution. We therefore do not account for these emissions which, although may be present, do not dominate the photometer light-curves.

Figure 3 shows the comparison between MMIA observed photometer signals and those calculated by using the proposed Equation 2 over the time after peak on a logarithmic scale. For short times after the emission, Equation 2 predicts a $\sim t^{-1/2}$ dependence for the flux that is cut off by either photon absorption with a time-scale τ_A or by the finite size of the source, with a time-scale τ_D. The cutoff from the mean absorption time is likely negligible: Luque et al. (2020) estimates $\tau_A \approx 2.3$ ms for clouds composed by water droplets with an effective radius of 20 μm and a droplet density of 10^8 m^{-3} but this possibly overestimates the absorption. The cloud tops are dominated by ice particles, which absorb radiation at 337 nm several orders of magnitude less efficiently than water (Warren & Brandt, 2008). Besides, the available estimates of the extinction coefficient

Table 2
Model-Inferred Properties of the Eight BLUE Events

ID	Cloud top height (km)	Cutoff time (τD) (ms)	Source length (L0) (km)	Optical energy at 337 nm (J)	Branching events
1	11.2	19.6[a]	–[a]	1.8×10^4	1.4×10^9
2	11.6	1.6	4.4	1.9×10^4	1.4×10^9
3	14.0	1.2	3.8	1.2×10^4	9.1×10^8
4	13.1	0.5	2.4	1.3×10^4	9.8×10^8
5	11.6	8.6[b]	–[b]	2.4×10^4	1.9×10^9
6	14.0	0.8	3.1	1.8×10^4	1.4×10^9
7	14.0	3.8[a]	–[a]	1.6×10^4	1.2×10^9
8	14.0	0.5	2.5	4.6×10^3	3.6×10^8

Note. We list the cloud top height measured by FY-4A at the event location, the best-fit cutoff time τ_D (See Equation 2 and Figure 3), the resulting source length $L_0 = (4D\tau_D)^{1/2}$ with $D = 3 \times 10^9$ m^2 s^{-1}, the total optical energy in the 337-nm band of the second positive system of nitrogen and an estimation of the number of streamer branching events in the fast breakdown processes that we assume that originated the events.

[a]In events 1 and 7, there is secondary activity that distorted the estimation of the cutoff time τ_D and the source length. [b]Event 5 has a light-curve that cannot be explained by an impulsive, uniformly bright source.

(Peterson, 2020; Platt, 1997) also lead to absorption times significantly longer than the duration of our events. Hence here we assume $\tau_A \gg \tau_D$.

As we show in Figure 3, most of the recorded BLUEs light-curves have the shape predicted by Equation 2. In the figure, we plot a least squares fit of the observational data to the model with two parameters: An overall amplitude factor and the decay time τ_D. To reduce the effect of the emissions from outside the cloud discussed above, we disregard the data points at the peak of the light-curve. The good fit of most events indicate that indeed they originate from sources that extend below the cloud top. Event 5 is the only one that does not show a clear $t^{-1/2}$ decay, possibly because there was a gap between the source and the cloud top or because light emissions were inhomogeneous or long-lasting. In events 1 and 7 there is weak secondary activity 1–2 ms after the main peak that distorts the estimate of the cutoff time τ_D.

From Table 2, leaving aside events where τ_D was estimated poorly, this cutoff time ranges between 0.5 and 1.6 ms. The smallest diffusion coefficient proposed by Soler et al. (2020), $D = 3 \times 10^9$ m^2 s^{-1} yields a range of lengths for the optical sources of $L_0 = 2.4$–4.4 km. However, the evaluated results will be affected by the uncertainties that surround our modeling of the cloud composition.

3.2. Monte Carlo Simulations

Next, we extend our model to include the propagation of the signal to the MMIA instruments, accounting for Rayleigh scattering by the atmosphere and for the non-isotropic (approximately Lambertian) emission pattern from the cloud tops. We use the radiative transfer Monte Carlo code CloudScat.jl (Luque et al., 2020) and run simulations of uniformly bright, straight vertical sources, with the lengths L_0 derived above, in a homogeneous cloud that spans altitudes from 7 km to the cloud top height derived by the Fengyun-4A (FY-4A) satellite

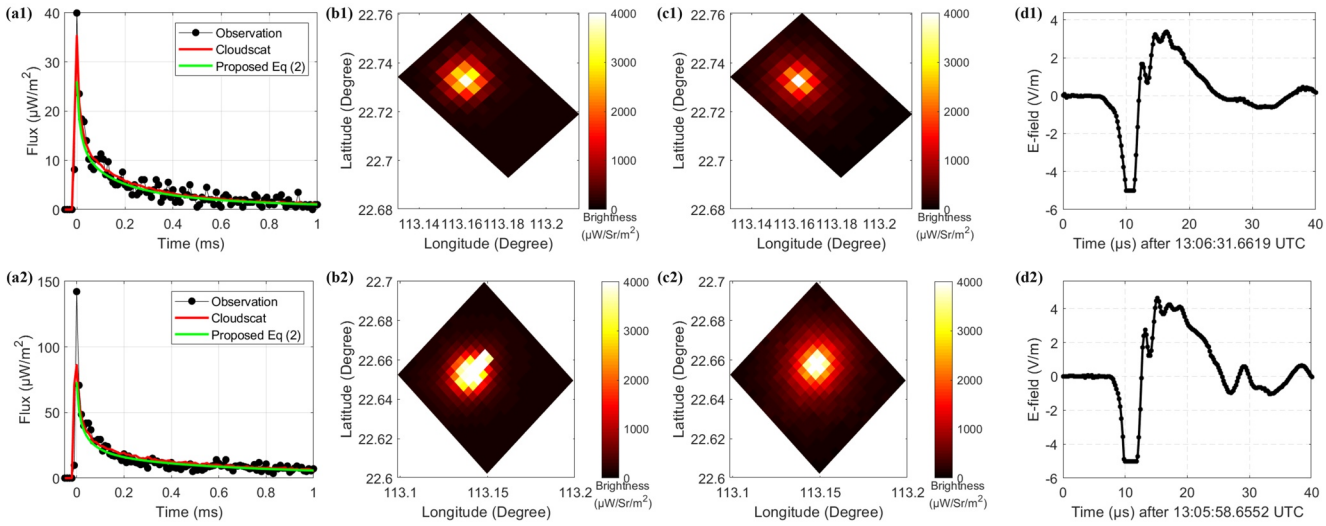

Figure 4. Comparing the modeling results against the observation of Modular Multispectral Imaging Array (MMIA) for event 8 (a1–d1) and event 2 (a2–d2). The 337 nm photometer signals (a1, a2): MMIA observation (black dotted line), modeling results by using CloudScat model (red line) and the proposed Equation 2 (green line). The images measured by 337 nm filtered camera of MMIA (b1, b2). The simulated images obtained from CloudScat model (c1, c2). The waveforms of the NBEs detected from the ground-based VLF/LF sensor at Guangzhou (d1, d2).

(listed in Table 2). The scattering parameters in the cloud are those for a density of 10^8 m^{-3} spherical ice particles with 20 μm radius. The relative positions between the source and the observer reproduce the conditions of each of the eight BLUEs in our data set. Note that the optical length L_0 in our study is a relative extension from the cloud top to a maximum depth. The uncertainties of the cloud top heights provided by FY-4A satellite do not affect the modeling results.

In Figure 4 we show the results of the Monte Carlo code comparing with 337-nm photometer and camera observations for the event 8 and 2 (Additional comparisons can be found in Figures S1–S8). The photometer light curves calculated from CloudScat model closely follow the analytical estimate of Equation 2 and are a good fit to the observations. The simulated camera images are also reasonably close to MMIA's records although they are slightly more compact. This is a possible indication of a non-negligible source width on the order of the camera resolution of about 400 m.

In the results presented here, we always consider that the top of the source coincides with the top of the cloud. As we discuss above, the effect of light emissions outside the cloud is too impulsive to compare against the MMIA photometer and is possibly dominated by the intrinsic time-dependence of the source. We performed additional Monte Carlo simulations that confirm that the photometer light-curves are compatible with source tops within a few hundred meters of the cloud top, either above or below it. The VLF/LF waveforms of negative NBEs for event 8 and 2 are also shown in Figure 4. The radio signals of the eight events, along with other positive NBEs at deeper locations in the same thunderstorm, are analyzed with more details in a complementary publication (F. Liu et al., 2021).

The CloudScat.jl code outputs a photon flux at the observer's location in units of photons per unit time and unit surface that reach a detector for each photon in the source whereas the MMIA photometers are calibrated in terms of power per unit surface (irradiance). The conversion factor is the total energy of the event in the 337-nm band, $E = Nhc/\lambda$, where N is the total number of photons emitted by the source, h is the Planck's constant, c is the speed of light and $\lambda = 337$ nm. By comparing the results of our Monte Carlo code to the MMIA data we found the best-matching total energy of each event. Because the events that we analyze are close to the cloud tops and thus barely affected by in-cloud absorption, our estimates of E are weakly sensitive to our model assumptions and thus provide a reasonably precise picture of the actual source emission intensity of the BLUE events. The estimated energies are listed in Table 2.

3.3. Streamer Branching Events

N. Liu et al. (2019) analyzed radio spectra of NBEs and concluded that they can be understood as systems of 10^7–10^8 streamers. In that analysis the key feature of a streamer is a current moment that increases rapidly on a time scale of about one nanosecond, which is the timescale of streamer initiation in numerical simulations. Here, in order to estimate the number of the streamer branching events for the BLUEs, we also consider that a single nanosecond event may produce more than one streamer, as is the case in a bifurcated tree. Denoting by b the mean number of streamers emerging from an event, we have $M = bK$, where M is the total number of streamers (unbifurcated branches) and K is the number of initiation events (most likely bifurcations from other streamers). Then the total streamer length contained in one fast breakdown process is ℓbK, where ℓ is the mean length between bifurcations (but see Nijdam et al., 2020 for a discussion of the difficulties involved in precisely defining this quantity). If a streamer emits η photons per unit length as it propagates, the total number of emitted photons is

$$N = \eta \ell b K. \tag{3}$$

The value of η depends on the air density. We first estimate its value at atmospheric density, η_0, by considering the numerical simulations by Malagón-Romero & Luque (2019). There we find a time-integrated photon yield of about $n_{\mathrm{ph}} = 2 \times 10^{18}$ m^{-3} in a streamer of radius $R \approx 2$ mm. The photon emission per unit length is then roughly

$$\eta_0 = \chi \pi R^2 n_{\mathrm{ph}}, \tag{4}$$

where, we have also included a factor χ that accounts for the fraction of emissions of the second positive system of N_2 inside the 5-nm window of the 337-nm MMIA photometer. From the spectra presented by Gordillo-Vázquez et al. (2012), we estimate $\chi \approx 0.3$. This leads to $\eta_0 \approx 8 \times 10^{12}\ m^{-1}$.

We now derive the photon yield η for a different air density n_{air} by applying the scaling laws for streamers (Ebert et al., 2010). A length such as R scales like n_{air}^{-1}. Because photons result from the electronic excitation of N_2 molecules into $N_2(C^3\Pi_u)$, their density n_{ph} is proportional to the electron density inside streamers, which scales as n_{air}^2. However the excited molecules are also collisionally quenched and the fraction of excited molecules that radiate is only

$$f = \frac{A}{A + k_1[N_2] + k_2[O_2]} = \frac{A}{A + k' n_{\mathrm{air}}}, \tag{5}$$

where A is the Einstein radiative coefficient, k_1 and k_2 are the rate coefficients for the quenching of the $N_2(C^3\Pi_u)$ state by collisions with, respectively, ground-state N_2 and O_2 and $k' = (k_1[N_2] + k_2[O_2])/n_{\mathrm{air}} \approx 0.8k_1 + 0.2k_2$. Capitelli et al. (2000) gives $A \approx 2 \times 10^7\ s^{-1}$, $k_1 \approx 10^{-17}\ \mathrm{m^3\ s^{-1}}$, $k_2 \approx 3 \times 10^{-16}\ \mathrm{m^3\ s^{-1}}$, which in our range of interest implies $k' n_{\mathrm{air}} \gg A$, leading to $f \approx A/k' n_{\mathrm{air}}$ (i.e., f scales as n_{air}^{-1}). Combining all factors we conclude that η scales as n_{air}^{-1}.

At an altitude of about 15 km, which is roughly the altitude of the events analyzed here, the air density is about 6 times lower than at ground value. The number of photons inside MMIA's 337-nm filter emitted by a streamer per unit length of propagation is about $\eta \approx 6\eta_0 = 5 \times 10^{13}\ \mathrm{m^{-1}}$.

To estimate the remaining factors in Equation 3, we first refer to Briels et al. (2008), who observed a ratio of branching length to streamer radius of about 20, so a radius of 2 mm at atmospheric pressure translates into $\ell \approx 6 \times 4\ \mathrm{cm} = 24\ \mathrm{cm}$ (Ebert et al., 2010). Finally, we take the branching number b to be 2, although there are evidences that it may possibly be slightly larger (Heijmans et al., 2013, 2015).

We can now solve for K in Equation 3 to find a number of branching events from the optical energies derived above. The results for all the BLUEs are listed in Table 2. Our results are 10–100 times above those derived from radio spectra by N. Liu et al. (2019). One possible reason for this disagreement is the uncertainties in our assumed parameters. For example, the estimated K is highly sensitive to the assumed streamer radius: had we chosen a radius of 5 mm at atmospheric pressure, the estimation of K would be reduced by about a factor 15. It is also possible that a large fraction of the optical signal in fast breakdown is emitted not close to streamer heads but from long-lived glows, as is the case in sprites (Luque et al., 2016; Pérez-Invernón et al., 2020).

Note, finally that our computations rely on extrapolations from streamer experiments and simulations at conditions that may turn to be different from those that prevail within a fast breakdown discharge inside a thundercloud. Nevertheless we find that the optical brightness of the BLUE events is compatible with an origin in extensive streamer coronas.

4. Discussion and Conclusions

The eight BLUE events that we analyze in this study expand and complete the picture of fast breakdown as the source of both optical blue-dominated emissions and radio pulses detected as NBEs in the VLF/LF bands or high-amplitude noise in VHF. All events were strongly detected in the photometer and camera filtred at 337 nm; in some events there was a weak signal in 180–230 nm but with no signal in 777.4 nm photometer and camera.

As in previous studies (Chanrion et al., 2017; Wescott et al., 1995; 1996), the BLUEs appeared temporally isolated from either CG or IC flashes detected by the GLD360 network. However, all the BLUEs coincide with NBEs observed by the ground-based VLF/LF sensor at Guangzhou. This strengthens the connection

between BLUEs and negative NBEs (Chou et al., 2018; F. Liu et al., 2018) and further supports that NBEs originate from non-thermal, streamer processes (Lyu et al., 2019; Rison et al., 2016; Tilles et al., 2019; Soler et al., 2020).

The rise times of the blue events in the 337 nm photometer are between 10 and 60 μs with peak irradiance varying from 20 to 140 μ Wm^{-2}. The brightness and short rise times suggest a source close or even slightly above the cloud tops and this is supported by our modeling results based either on the diffusion approximation by Koshak et al. (1994) or on a Monte Carlo radiative transfer code (Luque et al., 2020). Since all events are identified as negative NBEs, this is consistent with previous studies that place the initiation of most of negative NBEs between the upper positive charge region and the screening negative charge region of the thunderstorm (Lyu et al., 2015; Smith et al., 1999; Wu et al., 2012). The variation in the rise times between different events may be due to differences in the intrinsic time dependence of the optical sources but this is equally well explained by a finite distance to the cloud top or from nonuniformities of the optical sources below the cloud.

Our estimates of the total optical energy within the 337-nm band provide a new constraint for models of fast breakdown. The present understanding of these events is still limited and it is difficult to translate this energy into microscopical properties of fast breakdown. However our results confirm that fast breakdown involves more than 10^7 streamers, as inferred by N. Liu et al. (2019) and further analyzed by Cooray et al. (2020).

Future investigations should address the underlying physics of fast breakdown and its global significance, including its relation to lightning initiation. Data from the ASIM mission will likely play a decisive role in this research.

Appendix A: Constraints in the 777.4-nm Emission for Blue Luminous Events (BLUEs)

To establish rigorous bounds to the possible signal in the 777.4-nm photometer we proceed as follows. For each event first, we divide the photometer light-curve into temporal bins of $m = 40$ samples (0.4 ms) and compute the mean inside each bin b as

$$Y_b = \frac{1}{m} \sum_{i=k_b \ldots k_b+m-1} y_i, \tag{A1}$$

where k_b is the earliest sample inside b and y_i is the value of each sample. These $Y_b = S_b + \eta_b$ contain a possible signal from the observed events S_b as well as stochastic background noise η_b. To characterize the statistical distribution of η_b we find a bin where we can assume $S_b = 0$ by selecting the bin with the largest Y_b below the median of all Y_b. We compute the empirical average μ_1 and standard deviation σ_1 for the samples inside this background bin. Then we approximate the distribution function of η_b as a Gaussian with mean $\mu = \mu_1$ and standard deviation $\sigma = \sigma_1 / \sqrt{m}$. Hence we can mark bins with signals Y_b above $\mu + 3\sigma$ as statistically significant (p-value < 0.0014).

The fact that we do not have any statistically significant 777.4-nm observation coinciding with the 337-nm peaks implies that in all cases the 777.4-nm signal is, if it exists, weaker than $3\sigma \approx 0.1$ μW/m^2, which is between 200 and 1400 times below the different 337-nm peaks.

On the other hand, there are statistically significant emissions detected by the UV photometer sensitive to wavelengths in 180–230 nm. From our 8 events, 3 have UV detections coinciding with the 337-nm peaks at the 3σ level (events with ID 2, 3, and 5), 2 of them at the 5σ level (events with ID 4 and 6).

In Figure A1, we show the signals of the three photometers corresponding to event 6 in Tables 1 and 2 of the main text. This is the event with the strongest UV signal.

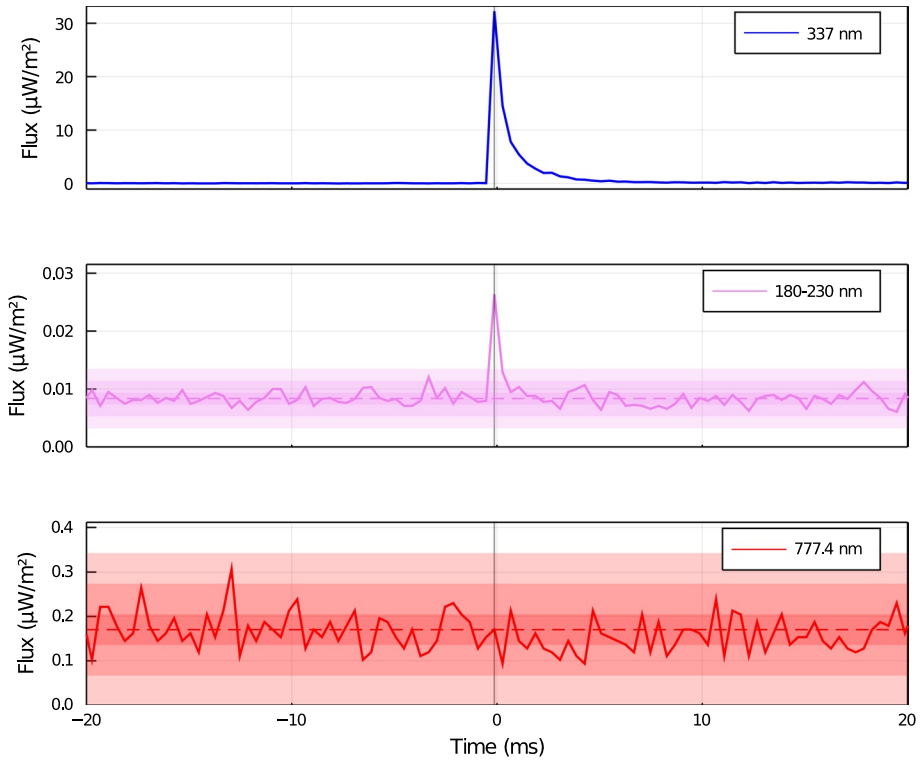

Figure A1. Signals from the three Modular Multispectral Imaging Array photometers for event 6, binned in intervals of 40 samples (0.4 ms). For 180–230 and 777.4 nm we also show an approximation to the background noise as described in the text: The horizontal, dashed line is the expected value μ and the shaded bands indicate $\mu \pm \sigma$, $\mu \pm 3\sigma$ and $\mu \pm 5\sigma$.

Appendix B: The Systematic Time Shift of MMIA With Respect to the Ground-Based Measurements

The systematic time shift of MMIA is estimated by using the 777-nm pulses and their simultaneous GLD360 events, which are (-23.3 ± 0.3) ms and (-6.2 ± 0.5) ms before and after the time adjustment τ, see Figure B1 for details.

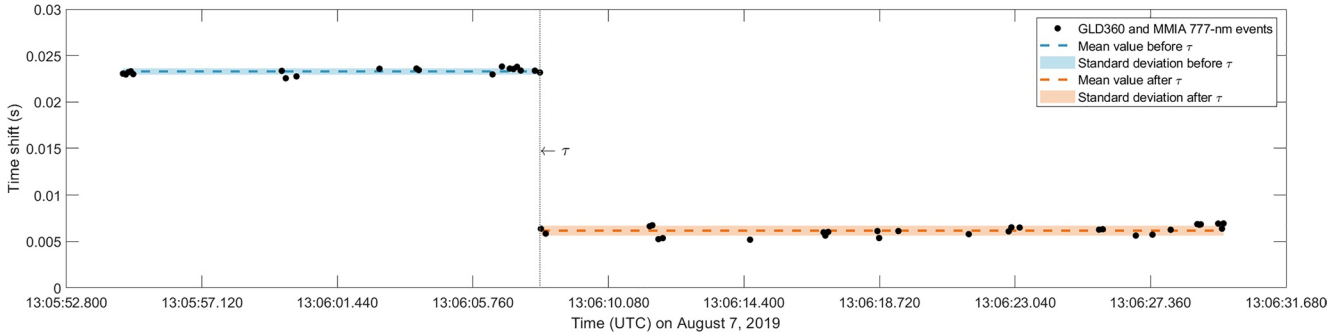

Figure B1. The systematic time shift of Modular Multispectral Imaging Array (MMIA) with respect to the ground-based measurements calculated by using MMIA 777-nm pulses and their simultaneous GLD360 events. The time shift experienced a time adjustment at τ around 13:06:07 (see black dashed line). The mean value before and after τ are −23.3 ms and −6.2 ms with the standard deviation ±0.3 ms and ±0.5 ms, respectively.

Data Availability Statement

The Modular Multispectral Imaging Array (MMIA) data and Global Lightning Detection Network GLD360 data used in this study were obtained at (https://asdc.space.dtu.dk/). The cloud top height data is based on the data sharing proxy in Fengyun Satellite data center (http://satellite.nsmc.org.cn/PortalSite/Data/Satellite.aspx?currentculture=en-US). The Himawari-8 gridded data in this study is supplied by the P-Tree System, Japan Aerospace Exploration Agency (JAXA)/Earth Observation Research Center (EORC) (https://www.eorc.jaxa.jp/ptree/). The data that support the findings of this study are openly available in (http://doi.org/10.5281/zenodo.4588549).

Acknowledgments
This work was supported by the European Research Council (ERC) under the European Union H2020 programme/ERC grant agreement 681257. It also received funding from the European Union Horizon 2020 research and innovation programme under the M. Sklodowska-Curie grant agreement SAINT 722337. Additionally, this work was supported by the Spanish Ministry of Science and Innovation, MINECO, under project PID2019-109269RB-C43 and FEDER program. D. Li, A. Luque and F. J. Gordillo-Vázquez acknowledge financial support from the State Agency for Research of the Spanish MCIU through the "Center of Excellence Severo Ochoa" award for the Instituto de Astrofísica de Andalucía (SEV-2017-0709). F. Liu, G. Lu and B. Zhu are supported by the National Key Research and Development Program of China (2017YFC1501501) and National Natural Science Foundation of China (41775004, 41875006, 42005068, U1938115).

References

Bandara, S., Marshall, T., Karunarathne, S., & Stolzenburg, M. (2021). Groups of narrow bipolar events within thunderstorms. *Atmospheric Research*, *252*, 105450. https://doi.org/10.1016/j.atmosres.2021.105450

Bessho, K., Date, K., Hayashi, M., Ikeda, A., Imai, T., Inoue, H., et al. (2016). An introduction to Himawari-8/9—Japan's new-generation geostationary meteorological satellites. *Journal of the Meteorological Society of Japan. Series II*, *94*(2), 151–183. https://doi.org/10.2151/jmsj.2016-009

Boeck, W. L., Vaughan, O. H., Blakeslee, R., Vonnegut, B., & Brook, M. (1998). The role of the space shuttle videotapes in the discovery of sprites, jets and elves. *Journal of Atmospheric and Solar-Terrestrial Physics*, *60*(7), 669–677. https://doi.org/10.1016/S1364-6826(98)00025-X

Briels, T. M. P., Veldhuizen, van, E. M., & Ebert, U. (2008). Positive streamers in air and nitrogen of varying density: Experiments on similarity laws. *Journal of Physics D: Applied Physics*, *41*(23), 234008. https://doi.org/10.1088/0022-3727/41/23/234008

Capitelli, M., Ferreira, C. M., Gordiets, B. F., & Osipov, A. I. (2000). *Plasma kinetics in atmospheric gases*. Berlin: Springer Verlag.

Chanrion, O., Neubert, T., Mogensen, A., Yair, Y., Stendel, M., Singh, R., & Siingh, D. (2017). Profuse activity of blue electrical discharges at the tops of thunderstorms. *Geophysical Research Letters*, *44*(1), 496–503. https://doi.org/10.1002/2016GL071311

Chanrion, O., Neubert, T., Rasmussen, I. L., Stoltze, C., Tcherniak, D., Jessen, N. C., et al. (2019). The modular multispectral imaging array (MMIA) of the ASIM payload on the international space station. *Space Science Reviews*, *215*(4), 1–25. https://doi.org/10.1007/s11214-019-0593-y

Chen, L., Zhang, Y., Lu, W., Zheng, D., Zhang, Y., Chen, S., & Huang, Z. (2012). Performance evaluation for a lightning location system based on observations of artificially triggered lightning and natural lightning flashes. *Journal of Atmospheric and Oceanic Technology*, *29*(12), 1835–1844. https://doi.org/10.1175/JTECH-D-12-00028.1

Chou, J. K., Hsu, R.-R., Su, H.-T., Chen, A. B.-C., Kuo, C.-L., Huang, S.-M., et al. (2018). ISUAL-observed blue luminous events: The associated sferics. *Journal of Geophysical Research: Space Physics*, *123*(4), 3063–3077. https://doi.org/10.1002/2017JA024793

Chou, J. K., Tsai, L. Y., Kuo, C. L., Lee, Y. J., Chen, C. M., Chen, A. B., et al. (2011). Optical emissions and behaviors of the blue starters, blue jets, and gigantic jets observed in the Taiwan transient luminous event ground campaign. *Journal of Geophysical Research*, *116*(A7). https://doi.org/10.1029/2010JA016162

Cooray, V., Cooray, G., Rubinstein, M., & Rachidi, F. (2020). Modeling compact intracloud discharge (CID) as a streamer burst. *Atmosphere*, *11*(5), 549. https://doi.org/10.3390/atmos11050549

Ebert, U., Nijdam, S., Li, C., Luque, A., Briels, T., & Veldhuizen, van, E. (2010). Review of recent results on streamer discharges and discussion of their relevance for sprites and lightning. *Journal of Geophysical Research*, *115*(A7). https://doi.org/10.1029/2009JA014867

Edens, H. E. (2011). Photographic and lightning mapping observations of a blue starter over a New Mexico thunderstorm. *Geophysical Research Letters*, *38*(17). https://doi.org/10.1029/2011GL048543

Gordillo-Vázquez, F. J., Luque, A., & Simek, M. (2012). Near infrared and ultraviolet spectra of TLEs. *Journal of Geophysical Research*, *117*(A5). https://doi.org/10.1029/2012JA017516

Gordillo-Vázquez, F. J., & Pérez-Invernón, F. J. (2021). A review of the impact of transient luminous events on the atmospheric chemistry: Past, present, and future. *Atmospheric Research*, *252*, 105432. https://doi.org/10.1016/j.atmosres.2020.105432

Heijmans, L. C. J., Clevis, T., Nijdam, S., Veldhuizen, Van, E., & Ebert, U. (2015). Streamer knotwilg branching: Sudden transition in morphology of positive streamers in high-purity nitrogen. *Journal of Physics D: Applied Physics*, *48*(35), 355202. https://doi.org/10.1088/0022-3727/48/35/355202

Heijmans, L. C. J., Nijdam, S., Veldhuizen, van, E. M., & Ebert, U. (2013). Streamers in air splitting into three branches. *EPL (Europhysics Letters)*, *103*(2), 25002. https://doi.org/10.1209/0295-5075/103/25002

Koshak, W. J., Solakiewicz, R. J., Phanord, D. D., & Blakeslee, R. J. (1994). Diffusion model for lightning radiative transfer. *Journal of Geophysical Research*, *99*(D7), 14361–14371. https://doi.org/10.1029/94JD00022

Krehbiel, P. R., Riousset, J. A., Pasko, V. P., Thomas, R. J., Rison, W., Stanley, M. A., & Edens, H. E. (2008). Upward electrical discharges from thunderstorms. *Nature Geoscience*, *1*(4), 233–237. https://doi.org/10.1038/ngeo162

Kuo, C.-L., Hsu, R. R., Chen, A. B., Su, H. T., Lee, L. C., Mende, S. B., et al. (2005). Electric fields and electron energies inferred from the ISUAL recorded sprites. *Geophysical Research Letters*, *32*(19). https://doi.org/10.1029/2005GL023389

Liu, B., Huo, J., Lyu, D., & Wang, X. (2021). Assessment of FY-4A and Himawari-8 cloud top height retrieval through comparison with ground-based millimeter radar at sites in Tibet and Beijing. *Advances in Atmospheric Sciences*, 1–17. https://doi.org/10.1007/s00376-021-0337-2

Liu, F., Lu, G., Neubert, T., Lei, J., Chanrion, O., Østgaard, N., et al. (2021). *Optical emissions associated with narrow bipolar events in radio signals from thunderstorm clouds penetrating into the stratosphere*. Research Square. https://doi.org/10.21203/rs.3.rs-311122/v110.21203/rs.3.rs-311122/v1

Liu, F., Zhu, B., Lu, G., Qin, Z., Lei, J., Peng, K.-M., et al. (2018). Observations of blue discharges associated with negative narrow bipolar events in active deep convection. *Geophysical Research Letters*, *45*(6), 2842–2851. https://doi.org/10.1002/2017GL076207

Liu, N., Dwyer, J. R., Tilles, J. N., Stanley, M. A., Krehbiel, P. R., Rison, W., et al. (2019). Understanding the radio spectrum of thunderstorm narrow bipolar events. *Journal of Geophysical Research: Atmosphere*, *124*(17–18), 10134–10153. https://doi.org/10.1029/2019JD030439

Luque, A., Gordillo-Vázquez, F. J., Li, D., Malagón-Romero, A., Pérez-Invernón, F. J., Schmalzried, A., et al. (2020). Modeling lightning observations from space-based platforms (Cloudscat.jl 1.0). *Geoscientific Model Development*, *13*(11), 5549–5566. https://doi.org/10.5194/gmd-13-5549-2020

Luque, A., Stenbaek-Nielsen, H. C., McHarg, M. G., & Haaland, R. K. (2016). Sprite beads and glows arising from the attachment instability in streamer channels. *Journal of Geophysical Research: Space Physics*, *121*(3), 2431–2449. https://doi.org/10.1002/2015JA022234

Lyons, W. A., Nelson, T. E., Armstrong, R. A., Pasko, V. P., & Stanley, M. A. (2003). Upward electrical discharges from thunderstorm tops. *Bulletin of the American Meteorological Society*, *84*(4), 445–454. https://doi.org/10.1175/BAMS-84-4-445

Lyu, F., Cummer, S. A., & McTague, L. (2015). Insights into high peak current in-cloud lightning events during thunderstorms. *Geophysical Research Letters*, *42*(16), 6836–6843. https://doi.org/10.1002/2015GL065047

Lyu, F., Cummer, S. A., Qin, Z., & Chen, M. (2019). Lightning initiation processes imaged with very high frequency broadband interferometry. *Journal of Geophysical Research: Atmosphere*, *124*(6), 2994–3004. https://doi.org/10.1029/2018JD029817

Malagón-Romero, A., & Luque, A. (2019). Spontaneous emergence of space stems ahead of negative leaders in lightning and long sparks. *Geophysical Research Letters*, *46*(7), 4029–4038. https://doi.org/10.1029/2019GL082063

Neubert, T., Chanrion, O., Heumesser, M., Dimitriadou, K., Husbjerg, L., Rasmussen, I. L., et al. (2021). Observation of the onset of a blue jet into the stratosphere. *Nature*, *589*(7842), 371–375. https://doi.org/10.1038/s41586-020-03122-6

Neubert, T., Østgaard, N., Reglero, V., Blanc, E., Chanrion, O., Oxborrow, C. A., et al. (2019). The ASIM mission on the international space station. *Space Science Reviews*, *215*(2), 1–17. https://doi.org/10.1007/s11214-019-0592-z

Nijdam, S., Teunissen, J., & Ebert, U. (2020). The physics of streamer discharge phenomena. *Plasma Sources Science and Technology*, *29*(10), 103001. https://doi.org/10.1088/1361-6595/abaa05

Pasko, V. P. (2008). Blue jets and gigantic jets: Transient luminous events between thunderstorm tops and the lower ionosphere. *Plasma Physics and Controlled Fusion*, *50*(12), 124050. https://doi.org/10.1088/0741-3335/50/12/124050

Pérez-Invernón, F. J., Malagón-Romero, A., Gordillo-Vázquez, F. J., & Luque, A. (2020). The contribution of sprite streamers to the chemical composition of the mesosphere-lower thermosphere. *Geophysical Research Letters*, *47*(14), e2020GL088578. https://doi.org/10.1029/2020GL08857810.1029/2020GL088578

Peterson, M. (2020). Modeling the transmission of optical lightning signals through complex 3-D cloud scenes. *Journal of Geophysical Research: Atmosphere*, *125*(23), e2020JD033231. https://doi.org/10.1029/2020JD033231

Platt, C. M. R. (1997). A parameterization of the visible extinction coefficient of ice clouds in terms of the ice/water content. *Journal of the Atmospheric Sciences*, *54*(16), 2083–2098. https://doi.org/10.1175/1520-0469(1997)054⟨2083:APOTVE⟩2.0.CO;2

Qin, Z., Zhu, B., Lyu, F., Ma, M., & Ma, D. (2015). Using time domain waveforms of return strokes to retrieve the daytime fluctuation of ionospheric D layer. *Chinese Science Bulletin*, *60*(7), 654–663.

Rison, W., Krehbiel, P. R., Stock, M. G., Edens, H. E., Shao, X.-M., Thomas, R. J., et al. (2016). Observations of narrow bipolar events reveal how lightning is initiated in thunderstorms. *Nature Communications*, *7*(1), 1–12. https://doi.org/10.1038/ncomms10721

Smith, D. A., Shao, X. M., Holden, D. N., Rhodes, C. T., Brook, M., Krehbiel, P. R., et al. (1999). A distinct class of isolated intracloud lightning discharges and their associated radio emissions. *Journal of Geophysical Research*, *104*(D4), 4189–4212. https://doi.org/10.1029/1998JD200045

Soler, S., Pérez-Invernón, F. J., Gordillo-Vázquez, F. J., Luque, A., Li, D., Malagón-Romero, A., et al. (2020). Blue optical observations of narrow bipolar events by ASIM suggest corona streamer activity in thunderstorms. *Journal of Geophysical Research: Atmosphere*, *125*(16), e2020JD032708. https://doi.org/10.1029/2020JD03270810.1029/2020JD032708

Surkov, V. V., & Hayakawa, M. (2020). Progress in the study of transient luminous and atmospheric events: A review. *Surveys in Geophysics*, *41*, 1101–1142. https://doi.org/10.1007/s10712-020-09597-2

Tilles, J. N., Liu, N., Stanley, M. A., Krehbiel, P. R., Rison, W., Stock, M. G., et al. (2019). Fast negative breakdown in thunderstorms. *Nature Communications*, *10*(1), 1–12. https://doi.org/10.1038/s41467-019-09621-z

Velde, van der, O. A., Montanyà, J., López, J. A., & Cummer, S. A. (2019). Gigantic jet discharges evolve stepwise through the middle atmosphere. *Nature Communications*, *10*(1), 1–10. https://doi.org/10.1038/s41467-019-12261-y

Warren, S. G., & Brandt, R. E. (2008). Optical constants of ice from the ultraviolet to the microwave: A revised compilation. *Journal of Geophysical Research*, *113*(D14). https://doi.org/10.1029/2007JD009744

Wescott, E. M., Sentman, D. D., Heavner, M. J., Hampton, D. L., Osborne, D. L., & Vaughan, Jr, O. H. (1996). Blue starters: Brief upward discharges from an intense Arkansas thunderstorm. *Geophysical Research Letters*, *23*(16), 2153–2156. https://doi.org/10.1029/96GL01969

Wescott, E. M., Sentman, D. D., Stenbaek-Nielsen, H. C., Huet, P., Heavner, M. J., & Moudry, D. R. (2001). New evidence for the brightness and ionization of blue starters and blue jets. *Journal of Geophysical Research*, *106*(A10), 21549–21554. https://doi.org/10.1029/2000JA000429

Wescott, E. M., Sentman, D., Osborne, D., Hampton, D., & Heavner, M. (1995). Preliminary results from the Sprites94 aircraft campaign: 2. blue jets. *Geophysical Research Letters*, *22*(10), 1209–1212. https://doi.org/10.1029/95GL00582

Wu, T., Dong, W., Zhang, Y., Funaki, T., Yoshida, S., Morimoto, T., et al. (2012). Discharge height of lightning narrow bipolar events. *Journal of Geophysical Research: Atmosphere*, *117*(D5). https://doi.org/10.1029/2011JD017054

Wu, T., Takayanagi, Y., Yoshida, S., Funaki, T., Ushio, T., & Kawasaki, Z. (2013). Spatial relationship between lightning narrow bipolar events and parent thunderstorms as revealed by phased array radar. *Geophysical Research Letters*, *40*(3), 618–623. https://doi.org/10.1002/grl.50112

Yang, J., Zhang, Z., Wei, C., Lu, F., & Guo, Q. (2017). Introducing the new generation of Chinese geostationary weather satellites, Fengyun-4. *Bulletin of the American Meteorological Society*, *98*(8), 1637–1658. https://doi.org/10.1175/BAMS-D-16-0065.1